Nanoscale

Accepted Manuscript

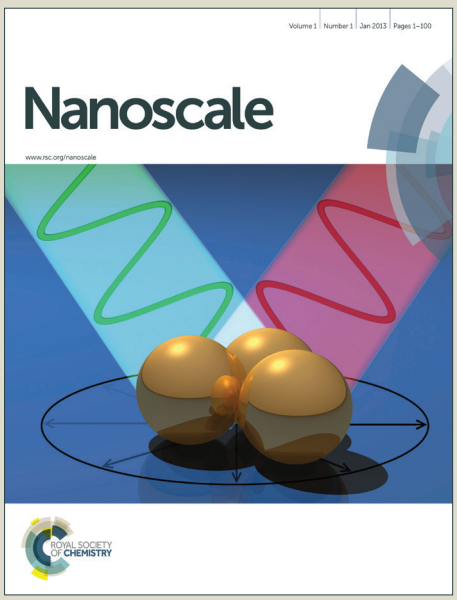

ROYAL SOCIETY OF CHEMISTRY

www.rsc.org/nanoscale

Journal Name

RSCPublishing

COMMUNICATION

DNA-based Detection of Mercury(II) Ions through Characteristic Current Signals in Nanopore with High Sensitivity and Selectivity

Cite this: DOI: 10.1039/x0xx00000x

Received 00th January 2012,
Accepted 00th January 2012

DOI: 10.1039/x0xx00000x

www.rsc.org/

Tao Zeng,[a,c] Ting Li,[a] Yuru Li,[a,d] Lei Liu,[a] Xingyong Wang,[d] Quansheng Liu,*[b] Yuliang Zhao,[a,c] Hai-Chen Wu*[a]

We report single-molecule detection of Hg^{2+} by threading a Hg^{2+} mediated DNA duplex through α-hemolysin nanopore which generates characteristic three-level current patterns enabling unambiguous detection of Hg^{2+}. This strategy precludes any background interference and features high sensitivity and selectivity. Besides, the platform could be readily integrated with aptamers and molecular beacons, offering extended possibilities for the construction of new DNA-based nanopore sensing system.

Introduction

Mercury pollution is a worldwide problem and has raised tremendous concerns. It originates from both natural incidents and anthropogenic resources, including volcano eruptions, gold mining, coal combustion, solid waste incineration, *etc*.[1] Due to the increasing human activities, mercury exposure has become a great threat to the environment and public health. Mercuric ion (Hg^{2+}), the most common form of mercury contamination in water, is neurotoxic[2] and causes damages to kidney[3] and immune system.[4] Moreover, inorganic mercury can be converted by bacteria into methylmercury,[5] which is then bioaccumulated through food chain[6] and leads to severe impairments to the neurological development of fetuses and children.[7] Consequently, a number of chemical sensors have been constructed for the sensitive detection of Hg^{2+}, by using organic chromogenic[8] and fluorogenic[9] probes, nanoparticles,[10] polymers,[11] DNA oligomers,[12] and so forth.

In the last two decades, nanopore technology has proved to be a powerful tool in single-molecule analysis and the detection of a variety of analytes, including small ions. Bayley's group constructed a couple of ion sensors based on engineered α-hemolysin (αHL) pores embedded with noncovalent[13] or covalent[14] binding sites. Gu and coworkers studied the effects of various alkaline and alkaline-earth cations on the dynamics of thrombin binding aptamer (TBA) trapped in αHL.[15] In one of our earlier work, we presented a stochastic Hg^{2+} sensing strategy in which a properly designed single-stranded DNA (ssDNA) probe was transformed into a hairpin structure upon Hg^{2+} binding whose translocation through αHL generated specific long-lived events that could be readily discerned from the 2D plot.[16] This system was able to detect Hg^{2+} at nanomolar concentration range. Later, a similar approach was employed for the simultaneous detection of Pb^{2+} and Ba^{2+} based on a G-quadruplex DNA.[17] Yet, to some extent this strategy suffers from the perturbation of randomly occurred long current blockades in the background when the transmembrane potential is elevated to gain high sensitivity. Guan and coworkers proposed an alternative where distinctive signals with intermediate current blockages were used to determine Hg^{2+}.[18] With the help of an engineered αHL, a detection limit of 25 nM was obtained. In this paper, we have developed a simple and highly sensitive DNA-based sensor for sensing Hg^{2+} in nanopore which effectively avoids the interference of background events and does not necessitate any protein engineering. With the mediation of Hg^{2+}, two rationally designed DNA strands with thymine-thymine (T-T) mismatches are assembled into a partial duplex structure which produces characteristic three-level current signatures when translocated through αHL nanopore, thus allowing Hg^{2+} identification with high confidence.

Results and Discussions

Design of DNA probes

Recently, Gu and coworkers reported that translocation of a hybrid of microRNA and probe DNA through αHL could produce multi-level signals when the hybrid dissociated and then progressively passed through the nanopore.[19] Inspired by their work, we speculated that a Hg^{2+} sensing probe could be obtained by properly designing a two-strand DNA probe mimicking the hybrid structure and substituting several natural base pairs with T-T mismatches (Fig. 1A). By reference to our previous hairpin-structured Hg^{2+} binding DNA,[16] we constructed the probe DNA1/DNA2 which contained four guanine-cytosine (G-C) pairs and seven T-T mismatches with additional poly$(dC)_{20}$ tails attached at both 3' and 5'-end of the DNA (Fig. S1). Indeed, upon the addition of Hg^{2+}, we observed the anticipated multi-level current events. However, its occurrence rate was as low as about 1 min^{-1}, along with a large number of single-level long blockades. We attributed this result to the inadequate length of DNA2 which might escape the nanopore from the *cis* side. Therefore, we attempted to elongate the short strand by adding noncomplementary overhangs (Fig. 1B) or increasing the number of

Table 1. List of the DNA sequences tested in this work.

Name	Sequence
DNA1	5'-$(C)_{20}$TTGTTTGTTGG$(C)_{20}$-3'
DNA2	5'-CCTTCTTTCTT-3'
DNA3	5'-$(C)_5$CCTTCTTTCTT$(C)_5$-3'
DNA4	5'-$(C)_{20}$TCTTGTGTCTCTGTTCG$(C)_{20}$-3'
DNA5	5'-CGTACTGAGTCTCTAGT-3'
P1	5'-ATGTTCTGTCG$(C)_{30}$-3'
P2	5'-CGTCTGATCAT$(C)_{30}$-3'
P3	5'-CGTCTGATCTT$(C)_{30}$-3'
P4	5'-CGTCAGATCAT$(C)_{30}$-3'
P5	5'-CGACTGAACAT$(C)_{30}$-3'
P6	5'-AGTTCTGTC$(C)_{30}$-3'
P7	5'-GTCTGATCT$(C)_{30}$-3'
P8	5'-ATCTGTC $(C)_{30}$-3'
P9	5'-GTCTGTT $(C)_{30}$-3'

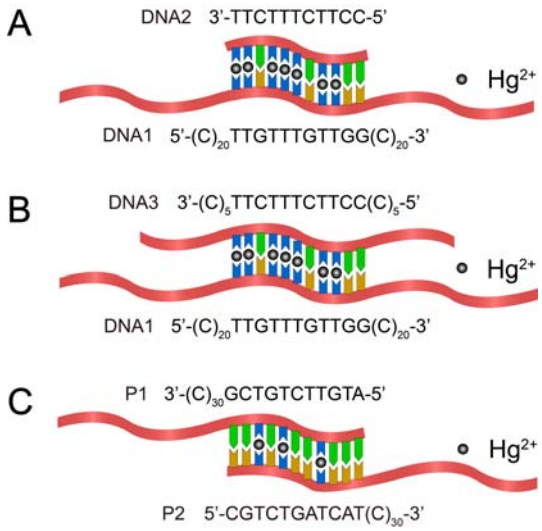

Fig. 1. Design of the DNA probes for sensing Hg^{2+}. (A) A T-Hg^{2+}-T containing DNA hybrid featuring a short strand paired with a long strand having tails at both ends. (B) Modified long-short DNA hybrid by attaching noncomplementary overhangs to both ends of the short strand. (C) A partial duplex of two 3'-tailed DNA strands mediated by natural base pairs and T-Hg^{2+}-T pairings. The sequences of the probes DNA1/DNA2, DNA1/DNA3, and P1/P2 are also given.

base pairings. Tagging both ends of DNA2 with a 5-C oligomer afforded DNA3 which paired with DNA1 for sensing Hg^{2+}; however, all the Hg^{2+}-specific signals disappeared (Fig. S2A). On the other hand, extending the Hg^{2+}-binding domain to seventeen base pairs (DNA4/DNA5) generated unexpected signature events in Hg^{2+}-free control group (Fig. S2B). These unsuccessful trials implied that it might be difficult to balance the number of base pairings and the length of the DNA probes by the initial design. Therefore, we decided to change the probe configuration by attaching the C_{30} tail to both DNAs at 3'-end (Fig. 1C). This would result in a partial duplex structure in the presence of Hg^{2+} with T-T mismatches and one C_{30} tail on each DNA. Translocation of such a hybrid through αHL would probably also generate characteristic current events and meanwhile circumvent the probe length problem. After optimization, we found that a pair of probe P1/P2 with eight Watson-Crick base pairs and three rationally inserted T-T mismatches gave the best results (Fig. 1C). The probe pair P1/P3 with seven natural base pairs and four T-T mismatches also gave high frequency of signature events but the presence of many ssDNA translocation events after incubation with Hg^{2+} indicated that the Hg^{2+}-binding efficiency of the probe was lower than P1/P2. Decreasing the numbers of T-T mismatches in the duplex region resulted in interferential signature events in the control groups (Fig. S4 and S5). Furthermore, it was rather surprising that we found the number of signature events drastically decreased or even completely vanished when we kept the three T-T mismatches and decreased the number of natural base pairs (Fig. S6). We reasoned that those natural base pairings might play important roles in initiating the duplex structures and without this process formation of T-Hg^{2+}-T became impossible.

Generation of signature events by P1-Hg^{2+}-P2

With the optimized probe P1/P2 in hand, we set out to comprehensively evaluate this strategy for Hg^{2+} detection. In the absence of Hg^{2+}, P1/P2 (1 μM final concentration for each DNA) only produced ssDNA translocation events (Fig. 2A and 2B). After incubation with 3 μM Hg^{2+} under the otherwise identical conditions, the anticipated characteristic three-level current signals were observed, with a frequency (f_{Hg}) of 8.9 ± 0.6 min^{-1} (Fig. 2C and 2D). The molecular mechanism of the translocation of P1-Hg^{2+}-P2 complex through αHL is illustrated in Fig. 2E, which agrees well with literature[19]. Level 1 represents the P1-Hg^{2+}-P2 hybrid entering the vestibule of αHL and then undergoing dissociation under the transmembrane potential. Level 2 corresponds to either P1 or P2 unzipped from the P1-Hg^{2+}-P2 complex temporally residing inside the nanocavity. The trapped probe is finally translocated through the β-barrel of αHL and produces a short-lived Level 3. The scatter plot of the Level 1 state of the signature events (normalized current blockage (I/I_0) *versus* event duration) is shown in Fig. 2F. The average current blockage of Level 1 is (87.5 ± 0.4)% of the open pore level (Fig. 2G), which is about 10% higher than ssDNA translocation events (Fig. S7). The average duration of Level 1 is 1757 ± 79 ms (Fig. 2H), which is significantly longer than that of the 22-base-pairing RNA-DNA hybrid presumably because the T-Hg^{2+}-T pairing is thermodynamically more stable than the natural base pairings, and thus requiring additional time for unzipping the Hg^{2+} stabilized duplex.[16,20] Level 2 is featured with a high residual current level and transient duration (440 ± 37 μs) compared with Level 1 (Fig. 2G and 2I). The current level of Level 3 dropped to about 87% blockage with an even shorter duration (91 ± 6 μs) than Level 2 (Fig. 2G and 2J). This value is comparable to that of ssDNA translocation through αHL. As it is known that nanopore-based sensing platforms are usually sensitive to the applied potentials, we moved on to investigate the performance of our system under different voltages. When the transmembrane potential was raised from +140 mV to +200 mV, the frequency of signature events increased by *ca.* 2.4 times and reached 30.2 ± 1.3 min^{-1} (Table S1). At the same time, the durations of Level 1 and Level 3 were significantly shortened along with the increase of voltages (Fig. S8). These observations supported the proposed physical explanation for the generation of three-level events, since elevation of the transmembrane potential would increase the capturing rate of the P1-Hg^{2+}-P2 complex and accelerate the dissociation and translocation of the complex. Other than the three-level signals, we also observed long-lived single-level blockades with residual currents (Fig. S9) resembling Level 1, which was ascribed to the trapped duplex escaping the nanocavity from the *cis* side[19] (Fig. 2C). The characteristic three-level pattern is

Journal Name RSCPublishing

COMMUNICATION

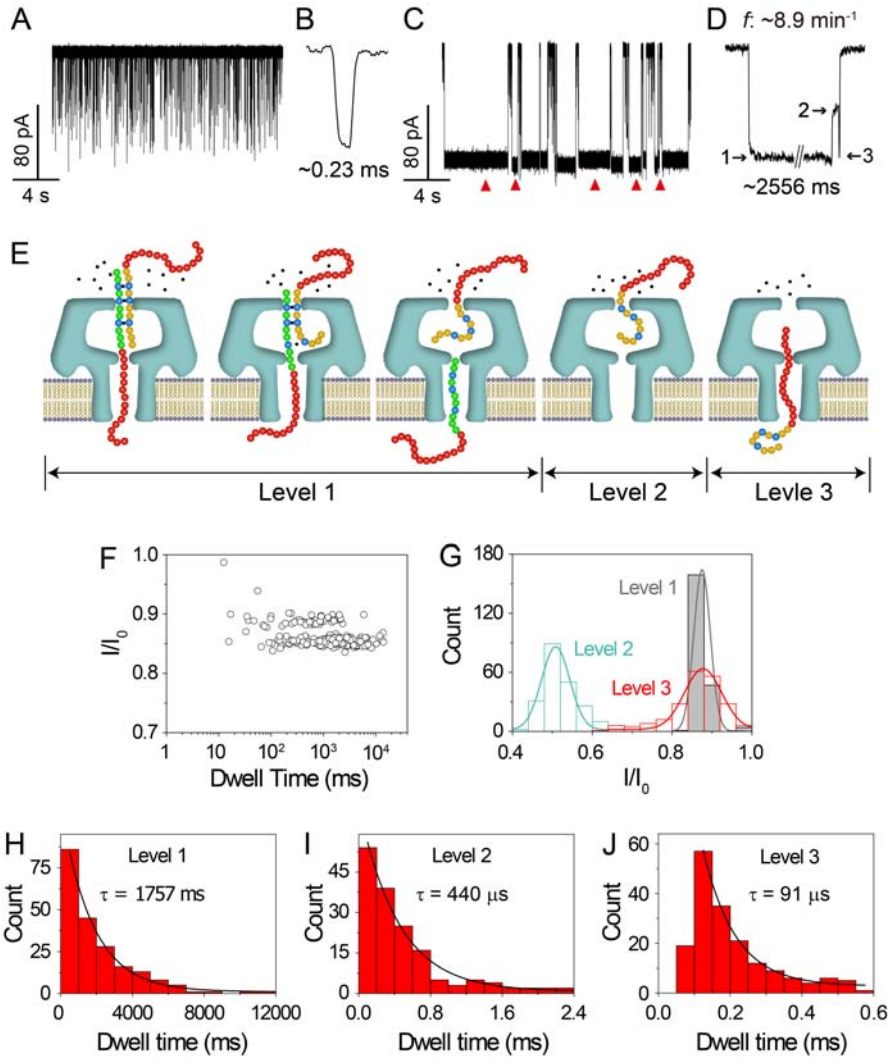

Fig. 2. Investigation of the events induced by probe P1/P2 with or without Hg^{2+}. (A) A representative single-channel current trace of the translocation of probe P1/P2 (1 μM final concentration for each DNA fragment) in the absence of Hg^{2+}. (B) Expanded view of a typical ssDNA translocation event. (C) A representative trace of the translocation of P1/P2 (1 μM final concentration for each fragment) in the presence of 3 μM Hg^{2+}. Red triangles denote the characteristic three-level blockades arising from the addition of Hg^{2+}. (D) Expanded view of a typical three-level signal. (E) Schematic illustration of the translocation of P1-Hg^{2+}-P2 complex through αHL. (F) Scatter plot of the Level 1 state of the Hg^{2+}-specific three-level events, plotted as normalized current blockage (I/I_0) *versus* event duration. (G) Histograms of the I/I_0 distribution of the three discrete levels indicated in D. Solid curves are Gaussian fit to the data. (H-J) Histograms of the dwell time distribution of the three levels. Data were fitted by a monoexponential decay function. All traces were recorded at +140 mV in the buffer of 1 M KCl and 10 mM Tris, pH 8.0, in the absence of presence of Hg^{2+}. Probe P1/P2 and Hg^{2+} were preincubated at 15 ± 2 ºC overnight before measurement. (number of individual experiments n = 6)

very useful in identifying Hg^{2+} in solution because all the background interference can be readily excluded. This property endows the new approach very high detection confidence.

Quantification of Hg^{2+}

Next, we explored the potential of our system for highly sensitive detection of Hg^{2+}. We employed an asymmetrical salt condition to lower the detection limit, as successfully demonstrated in our previous work and other reports.[16,19,20] Initially, a gradient of *trans* 3 M KCl/*cis* 0.15 M KCl was attempted. However, under this condition data collection was interrupted by high frequency of permanent clogging after Hg^{2+} exposure, due to the long-time trap of P1-Hg^{2+}-P2 complex in the nanopore (Fig. S10A). This issue was then resolved by decreasing the gradient to *trans* 3 M KCl/*cis* 0.5 M KCl, which

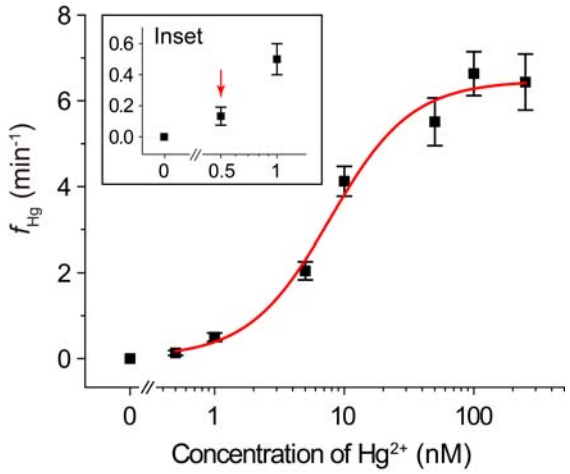

Fig. 3. Quantification of Hg^{2+}. Plot of the frequency of Hg^{2+}-related three-level signal (f_{Hg}) *versus* Hg^{2+} concentration. Experiments were conducted in asymmetrical KCl solutions, 3 M *trans*/0.5 M *cis*, buffered with 10 mM Tris, pH 8.0 with the transmembrane potential held at +140 mV. DNA probe P1/P2 (10 nM final concentration for each DNA fragment) was preincubated with 0, 0.5, 1.0, 5, 10, 50, 100, and 250 nM of Hg^{2+} respectively at 15 ± 2 ºC overnight. The data could be fitted by a Boltzmann fitting, $f_{Hg} = 6.46 - 6.43/(1 + \exp((\log[Hg^{2+}] - 0.89)/0.31))$. The detection limit was determined to be 0.5 nM, as indicated by the red arrow (inset). (number of individual experiments n = 3)

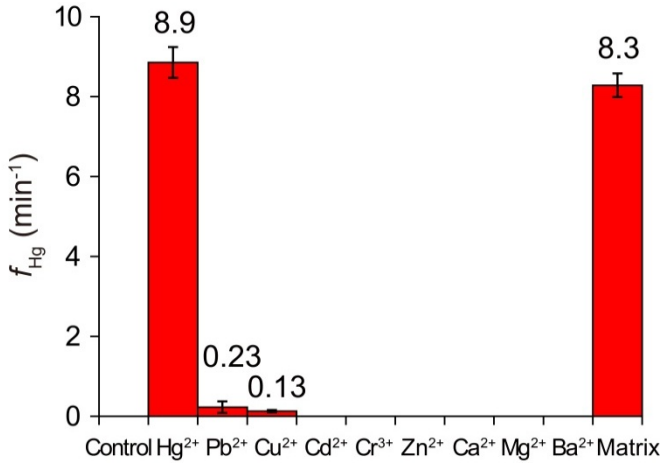

Fig. 4. Selectivity study. Comparison of f_{Hg} when P1/P2 was exposed to Hg^{2+}, Pb^{2+}, Cu^{2+}, Cd^{2+}, Cr^{3+}, Zn^{2+}, Ca^{2+}, Mg^{2+}, Ba^{2+}, and an analyte matrix. All metal ions were tested at a concentration of 3 μM. The matrix was composed of Hg^{2+} and all other interfering metal ions. Data were acquired at +140 mV in the buffer of 1 M KCl and 10 mM Tris, pH 8.0. DNA probe P1/P2 (1 μM final concentration for each DNA fragment) was incubated with individual metal ions or analyte matrix at 15 ± 2 ºC overnight before measurement. (number of individual experiments n = 3)

had little influence on the generation of signature events (Fig. S10B). Therefore we selected this condition for the determination of low concentration of Hg^{2+}. The probe concentration used in these experiments was 10 nM for each DNA strand. As shown in Fig. 3, in the range of 0.5 nM to 100 nM of Hg^{2+}, the f_{Hg} rose monotonically with the increase of Hg^{2+} amount, and the data could be fitted by a Boltzmann fitting, $f_{Hg} = 6.46 - 6.43/(1 + \exp((\log[Hg^{2+}] - 0.89)/0.31))$. No further increase of f_{Hg} was observed when the Hg^{2+} concentration exceeded 100 nM. Owing to the clean background, we could confirm the existence of Hg^{2+} at 0.5 nM (indicated by the red arrow, Fig. 3 inset), which afforded a f_{Hg} of 0.13 ± 0.03 min^{-1} that was statistically separated from the control group whose f_{Hg} was 0 ($p < 0.01$ in t-test). The detection limit for Hg^{2+} could be further improved by simply increasing the applied transmembrane potential, which was not feasible in our previous work because the elevated voltage might reduce the detection confidence due to the background events.[16]

Selectivity study

Finally, we evaluated the specificity of this Hg^{2+} sensor. Experiments were first carried out by incubating probe P1/P2 (1 μM final concentration for each fragment) with 3 μM of individual interfering metal ions, including Pb^{2+}, Cu^{2+}, Cd^{2+}, Cr^{3+}, Zn^{2+}, Ca^{2+}, Mg^{2+}, Ba^{2+}. The results indicated that these metal ions had no inteference with Hg^{2+} sensing, except for Pb^{2+} and Cu^{2+} which occasionally generated very few interfering three-level events. The comparisons of f_{Hg} are listed in Fig. 4. Moreover, the detection of Hg^{2+} was further challenged in an analyte matrix containing all tested ions. The f_{Hg} decreased by less than 10% as compared with the value obtained in the presence of 3 μM of Hg^{2+} alone (Fig. 4). Hence, the DNA probe is confirmed to have high selectivity towards Hg^{2+}.

Conclusions

In this work, we have demonstrated a new nanopore sensor for the single-molecule detection of Hg^{2+} by taking the advantage of the characteristic current pattern derived from a Hg^{2+} mediated DNA assembly traversing αHL. In the presence of Hg^{2+}, two rationally designed 3'-tailed DNA strands containing eight natural base pairings and three T-T mismatches, namely probe P1/P2, forms a stable duplex through thymine-Hg^{2+} interactions and generates specific three-level signature events for Hg^{2+} recognition when translocated through αHL. This feature precludes any interference from background noise, making the sensor highly sensitive for Hg^{2+}, with a detection limit of ~0.5 nM. At the same time, the platform has a superior selectivity towards Hg^{2+} over other interfering metal ions and thus could be potentially applied to real samples. Another advantage of the system is that it uses commercially available wildtype αHL and no probe labelling is required. Furthermore, this strategy could be combined with the design of DNA aptamers and molecular beacons to construct new nanopore sensing systems.

Experimental section

Materials

All oligonucleotides were purchased from Tsingke Technologies (Beijing, China) and purified by PAGE. Wild type αHL was prepared as previously described.[16] 1,2-Diphytanoyl-sn-glycero-3-phosphocholine (DPhPc) was purchased from Avanti Polar Lipids (Alabaster, Alabama). All other chemicals were of high purity and used as received.

Single-channel recording

The DPhPc lipid bilayer was formed over a 100-150 μm aperture drilled in a 20-μm thick polycarbonate film (Goodfellow, Malvern, PA) that divided the chamber into *cis* and *trans* compartments. Both compartments contained 1 mL buffer of 1 M KCl and 10 mM Tris, pH 8.0, unless otherwise stated. αHL was inserted from the *cis* side. Traces were recorded at a sampling frequency of 100 kHz and filtered with a low-pass Bessel filter operating at 5 kHz (Axon Instruments, Foster City, CA). In voltage study experiments, the cut-off frequency was increased to 10 kHz to prevent the events from being under sampled. DNA probes were preincubated with Hg^{2+} and other interfering metal ions overnight at 15 ± 2 ºC before measurement. All experiments were conducted at 15 ± 2 ºC.

Data analysis

Current traces were analyzed with Clampfit 10.2 software (Axon Instruments). The three-level events were manually picked. Origin (Microcal, Northampton, MA, version 8.5) and Clampfit 10.2 were used for graph construction and curve fitting. Adobe Illustrator (Adobe Systems Incorporated, San Jose, CA) was used to make figures. All scatter plots and histograms were constructed based on at least 200 events.

Acknowledgements

This research was supported by the National Natural Science Foundation of China (no. 21205119 and 21175135), the National Basic Research program of China (973 program, no. 2010CB933600), and the "100 Talents" program of the Chinese Academy of Sciences.

Notes and references

[a] *Key Laboratory for Biomedical Effects of Nanomaterials & Nanosafety,*
[b] *Multidisciplinary Center, Institute of High Energy Physics, Chinese Academy of Sciences, Beijing 100049, China. Fax: +86 10 88235745; Tel: +86 10 88235745; E-mail: haichenwu@ihep.ac.cn.*
[c] *National Center for Nanoscience and Technology of China, Beijing 100190, China.*
[d] *School of Chemical Engineering, University of Mining & Technology, Xuzhou 221116, Jiangsu, China*

1. UNEP, Global Mercury Assessment 2013: Sources, Emissions, Releases and Environmental Transport. UNEP Chemicals Branch, Geneva, Switzerland, 2013.
2. L. W. Chang, *Environ Res*, 1977, **14**, 329-373.
3. R. K. Zalups and S. Ahmad, *J Am Soc Nephrol*, 2004, **15**, 2023-2031.
4. E. K. Silbergeld, I. A. Silva and J. F. Nyland, *Toxicol Appl Pharm*, 2005, **207**, 282-292.
5. M. K. Hamdy and O. R. Noyes, *Appl Microbiol*, 1975, **30**, 424-432.
6. A. Renzoni, F. Zino and E. Franchi, *Environ Res*, 1998, **77**, 68-72.
7. (a) G. E. Mckeowneyssen, J. Ruedy and A. Neims, *Am J Epidemiol*, 1983, **118**, 470-479; (b) P. W. Davidson, G. J. Myers, C. Cox, C. F. Shamlaye, D. O. Marsh, M. A. Tanner, M. Berlin, J. SloaneReeves, E. Cernichiari, O. Choisy, A. Choi and T. W. Clarkson, *Neurotoxicology*, 1995, **16**, 677-688; (c) P. Grandjean, P. Weihe, R. F. White and F. Debes, *Environ Res*, 1998, **77**, 165-172.
8. (a) E. Coronado, J. R. Galan-Mascaros, C. Marti-Gastaldo, E. Palomares, J. R. Durrant, R. Vilar, M. Gratzel and M. K. Nazeeruddin, *J Am Chem Soc*, 2005, **127**, 12351-12356; (b) S. Tatay, P. Gavina, E. Coronado and E. Palomares, *Org Lett*, 2006, **8**, 3857-3860.
9. (a) S. K. Ko, Y. K. Yang, J. Tae and I. Shin, *J Am Chem Soc*, 2006, **128**, 14150-14155; (b) E. M. Nolan and S. J. Lippard, *J Am Chem Soc*, 2007, **129**, 5910-5918; (c) S. Ando and K. Koide, *J Am Chem Soc*, 2011, **133**, 2556-2566.
10. (a) J. S. Lee, M. S. Han and C. A. Mirkin, *Angew Chem Int Edit*, 2007, **46**, 4093-4096; (b) R. Freeman, T. Finder and I. Willner, *Angew Chem Int Edit*, 2009, **48**, 7818-7821; (c) F. Xia, X. L. Zuo, R. Q. Yang, Y. Xiao, D. Kang, A. Vallee-Belisle, X. Gong, J. D. Yuen, B. B. Y. Hsu, A. J. Heeger and K. W. Plaxco, *P Natl Acad Sci USA*, 2010, **107**, 10837-10841.
11. (a) I. B. Kim and U. H. F. Bunz, *J Am Chem Soc*, 2006, **128**, 2818-2819; (b) X. F. Liu, Y. L. Tang, L. H. Wang, J. Zhang, S. P. Song, C. H. Fan and S. Wang, *Adv Mater*, 2007, **19**, 1471-1474.
12. (a) A. Ono and H. Togashi, *Angew Chem Int Edit*, 2004, **43**, 4300-4302; (b) M. Hollenstein, C. Hipolito, C. Lam, D. Dietrich and D. M. Perrin, *Angew Chem Int Edit*, 2008, **47**, 4346-4350.
13. (a) O. Braha, L. Q. Gu, L. Zhou, X. F. Lu, S. Cheley and H. Bayley, *Nat Biotechnol*, 2000, **18**, 1005-1007; (b) S. Cheley, L. Q. Gu and H. Bayley, *Chem Biol*, 2002, **9**, 829-838.
14. S. H. Shin, T. Luchian, S. Cheley, O. Braha and H. Bayley, *Angew Chem Int Edit*, 2002, **41**, 3707-3709.
15. J. W. Shim, Q. L. Tan and L. Q. Gu, *Nucleic Acids Res*, 2009, **37**, 972-982.
16. S. Wen, T. Zeng, L. Liu, K. Zhao, Y. L. Zhao, X. J. Liu and H. C. Wu, *J Am Chem Soc*, 2011, **133**, 18312-18317.
17. C. Yang, L. Liu, T. Zeng, D. W. Yang, Z. Y. Yao, Y. L. Zhao and H. C. Wu, *Anal Chem*, 2013, **85**, 7302-7307.
18. G. H. Wang, Q. T. Zhao, X. F. Kang and X. Y. Guan, *J Phys Chem B*, 2013, **117**, 4763-4769.
19. Y. Wang, D. L. Zheng, Q. L. Tan, M. X. Wang and L. Q. Gu, *Nat Nanotechnol*, 2011, **6**, 668-674.
20. Y. Miyake, H. Togashi, M. Tashiro, H. Yamaguchi, S. Oda, M. Kudo, Y. Tanaka, Y. Kondo, R. Sawa, T. Fujimoto, T. Machinami and A. Ono, *J Am Chem Soc*, 2006, **128**, 2172-2173.
21. M. Wanunu, W. Morrison, Y. Rabin, A. Y. Grosberg and A. Meller, *Nat Nanotechnol*, 2010, **5**, 160-165.